Dalton Transactions

ROYAL SOCIETY OF CHEMISTRY

PAPER

View Article Online
View Journal | View Issue



Cite this: *Dalton Trans.*, 2024, **53**, 5711

# Coordination chemistry of alkali metal dimesityl-thio- and dimesityl-selenophosphinites $[(L)_2A\text{-}EPMes_2]_2$ (A = Li, Na, K; E = S, Se; L = THF, THP) and $[(18C6)K\text{-}SPMes_2]$†

Richard C. C. Dorow, Phil Liebing, Helmar Görls and Matthias Westerhausen *

The reactions of dimesitylphosphane oxide $Mes_2P(O)H$ with Lawessons reagent and dimesitylphoshane with selenium yield $Mes_2P(E)H$ with E = S (**1a**) and E = Se (**1b**), respectively, with moderate yields. Metalation of dimesitylphosphane sulfide **1a** with *n*-butyllithium, sodium hydride or potassium hydride in THF allows the isolation of dinuclear dimesityl-thiophosphinites of the type $[(thf)_2A\text{-}S\text{-}PMes_2]_2$ [A = Li (**4**), Na (**5**), K (**2a**)] with central four-membered $A_2S_2$ rings. The weaker base THP leads to the very similar aggregate $[(thp)_2K\text{-}S\text{-}PMes_2]_2$ (**3a**) as has also been observed for the homologous potassium dimesityl-selenophosphinites of the type $[(L)_2K\text{-}Se\text{-}PMes_2]_2$ [L = thf (**2b**), thp (**3b**)]. Addition of 18-crown-6 ether leads to deaggregation and expectedly to formation of mononuclear $[(18C6)K\text{-}S\text{-}PMes_2]$ (**6**). Moderate yields have been obtained due to dismutation reactions that yield the corresponding phosphinates $AE_2PMes_2$ and phosphanides $APMes_2$, a degradation process which has been observed earlier also for Li-O-$PMes_2$. This side reaction hampers the application of these thio- and selenophosphinites as catalysts in the addition of phosphane sulfides and selenides across alkynes.

Received 29th January 2024,
Accepted 28th February 2024

DOI: 10.1039/d4dt00264d

rsc.li/dalton



## Introduction

Diarylphosphane oxides $Ar_2P(O)H$ are an important substance class for the formation of P–C, P–O and P–N bonds yielding tertiary phosphane oxides of the type $Ar_2P(O)R$ (Ar = aryl, R = alkyl, aryl, H).[1] Often the P–H functionality lacks reactivity and drastic reaction conditions and/or activation of these secondary phosphane oxides by substitution of the P-bound hydrogen atom by an electropositive metal are required for the addition of the P–H bond onto alkenes and alkynes. Metalation of these phosphane oxides yields diarylphosphinites of the type M-O-$PAr_2$; electropositive metals such as alkali and alkaline-earth metals are bound at the oxygen atom and the P atom is in a trigonal-pyramidal environment. Decreasing electronegativity and increasing softness of the s-block metal ions are beneficial for catalytic addition of $Ar_2P(O)H$ across alkynes.[2] Thus, heavy alkali metal phosphinite catalysts $Ar_2P\text{-}O\text{-}A$ (especially of the softer alkali metals A like potassium, rubidium and cesium) are the preferred choice for quantitative conversion of diarylphosphane oxides and alkynes into alkenyl-diarylphosphane oxides (Scheme 1) whereas small and hard alkaline-earth metal congeners (especially of magnesium and calcium) show no catalytic activity. In addition, heterobimetallic alkali metal/magnesium phosphinite complexes proved to be very reactive in this hydrophosphorylation reaction, too.[3]

The instability in solution of some alkali metal phosphinites has been recognized; thus, lithium dimesitylphosphinite Li-$OPMes_2$ dismutates into lithium phosphinate $Li(O_2PMes_2)$ and lithium phosphanide $LiPMes_2$ (Scheme 2).[4] This degradation process can be prevented by coordination of soft cadmium species to the free electron pairs of the phosphorus atoms. Contrary to the hydrogen atom, the alkali metal ions are always bonded to the hard oxygen base and at the phosphorus site, a soft free electron pair is available for coordi-

*Friedrich Schiller University Jena, Institute of Inorganic and Analytical Chemistry, Humboldtstraße 8, D-07743 Jena, Germany. E-mail: m.we@uni-jena.de*

†Electronic supplementary information (ESI) available: NMR and IR spectra as well as the molecular structure of **1b**. CCDC 2184155 for **1a**, 2184156 for **1b**, 2184157 for **2a**, 2184158 for **2b**, 2184159 for **3a**, 2184160 for **3b**, 2184161 for **4**, 2184162 for **5**, 2184163 for **(tmeda)NaOPMes$_2$**, and 2254279 for **6**. For ESI and crystallographic data in CIF or other electronic format see DOI: https://doi.org/10.1039/d4dt00264d

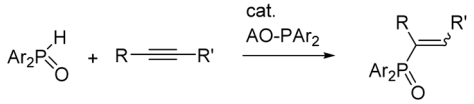


**Scheme 1** Catalytic hydrophosphorylation of alkynes with diarylphosphane oxides in the presence of catalytic amounts of AO-$PAr_2$ (Ar = aryl).

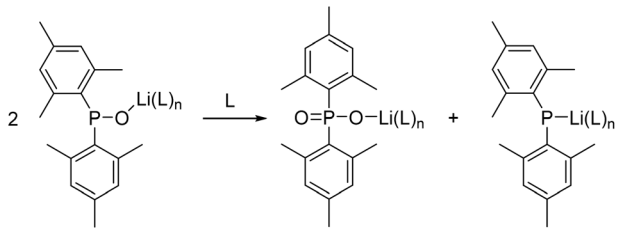


**Scheme 2** Dismutation of dissolved lithium dimesitylphosphinite in solvent L yielding lithium dimesitylphosphinate and lithium dimesitylphosphanide. Possible aggregation and deaggregation equilibria in solution are neglected.

nation chemistry to soft (transition) metals.[5] Despite the reactivity, tetranuclear [(thf)Li-OPPh$_2$]$_4$ and dinuclear [(dme)Li-OPPh$_2$]$_2$ with tetra-coordinate lithium atoms have been isolated and structurally authenticated.[6,7]

Potassium diarylphosphinites crystallize as tetranuclear complexes with central $K_4O_4$ heterocubane cages, the tetra-coordination of the oxygen bases decelerates dismutation processes which have been observed for the lithium derivatives.[8] Despite these challenges, alkali metal phosphinites have been known for a long time.[9] NMR studies verify that in solution the phosphinite ions bind *via* the oxygen atom to the alkali metals.[10–12] A similar coordination behavior has been observed for the homologous diphenyl-thiophosphinites of lithium, sodium and potassium.[11] Heavier diaryl-chalcogenophosphinites have also been studied by NMR spectroscopy.[10,12] In general, these alkali metal phosphinites are accessible by two different strategies: (i) reduction of chloro-diarylphosphane oxides with s-block metals and (ii) deprotonation of diarylphosphane oxides with alkali metal hydrides or organometallics.

Diphenylphosphane oxide (P–O 148.81(11) pm),[13] sulfide (P–S 195.60(7) pm)[8] and selenide (P–Se 211.27(9) pm)[14] have very similar molecular structures due to lack of steric pressure. Slight differences arise from a significantly larger electronegativity difference for the oxide (Allred-Rochow electronegativity values: P 2.06, O 3.50, S 2.44, Se 2.48)[15] making the P atom more positive. The C–P–C bond angle of 108.40(7)° and the P–C bond lengths (179.82(15) and 180.15(14) pm)[13] for Ph$_2$P(O)H differ only slightly from the values for Ph$_2$P(S)H (C–P–C 105.97(9)°, P–C 180.7(2) and 181.1(2) pm)[8] and Ph$_2$P(Se)H (C–P–C 107.56(14)°, P–C 180.4(3) and 181.0(3) pm).[14] Deprotonation and formation of diphenylphosphinites[6,7] and diphenyl-thiophosphinites[8] lead to significant elongation of the P–O and P–S bonds. In addition, [(thp)K-SPPh$_2$]$_\infty$ crystallizes with a unique wavy strand structure.[8]

The properties of diarylphosphinites strongly depend on the chalcogen (electronegativity, radius) and on the alkali metal (electronegativity, radius, surface charge density, hardness) and therefore, we started our investigation with K-SPMes$_2$ to compare this complex with well-studied K-OPMes$_2$ [8] and K-SPPh$_2$ [8] and varied the chalcogen as well as alkali metal atom to elucidate their influence on NMR and structural parameters.

# Results and discussion

## Synthetic procedures

We chose mesityl-substituted chalcogenophosphinites due to beneficial crystallization behavior and enhanced stability with respect to dismutation into phosphinates and phosphanides as had been observed for Li-OPMes$_2$ yielding LiPMes$_2$ and LiO$_2$PMes$_2$.[4] Thus, the structure of [(18C6)K-OPPh$_2$] was impaired by cocrystallization with the phosphinate [(18C6)K-O$_2$PPh$_2$] whereas an analytically pure, crystalline sample of [(18C6)K-OPMes$_2$] was studied for the derivative with the bulkier mesityl substituents.[16]

An advantageous straightforward synthesis of potassium dimesityl-chalcogenophosphinites was the deprotonation of the dimesitylphosphane chalcogenides with potassium hydride as depicted in Scheme 3.

For the elucidation of the structural influence of the alkali metal, lithium and sodium dimesityl-thiophosphinites were included in this investigation. Metalation of Mes$_2$P(S)H (**1a**) succeeded smoothly in THF with *n*BuLi or NaH yielding lithium (**4**) and sodium dimesityl-thiophosphinites (**5**), respectively, as shown in Scheme 4.

All these dimesityl-chalcogenophosphinites crystallized as dinuclear molecules. The bulky mesityl groups hinder aggregation and formation of coordination polymers. The dinuclear complexes deaggregated after addition of a stoichiometric

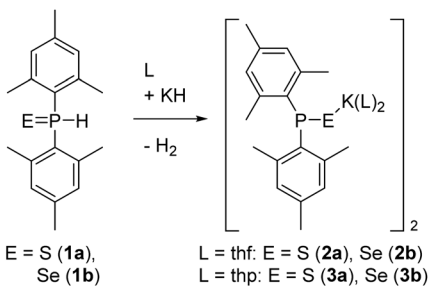


**Scheme 3** Synthesis of thf (**2**) and thp (**3**) adducts of potassium dimesityl-chalcogenophosphinites *via* metalation of dimesitylphosphane chalcogenides (E = S (**a**), Se (**b**)) with potassium hydride in an ethereal solvent L (L = THF, THP).

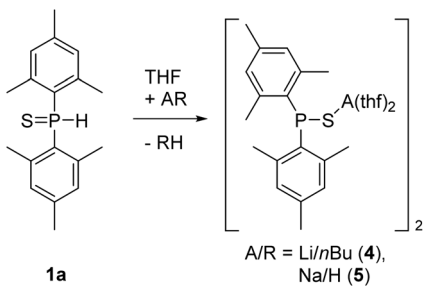


**Scheme 4** Synthesis of thf adducts of lithium and sodium dimesityl-thiophosphinites (**4**, **5**) *via* metalation of dimesitylphosphane sulfide (**1a**) with *n*BuLi and NaH in THF.

amount of [18]crown-6 yielding yellow mononuclear [(18C6)K-SPMes$_2$] (**6**) as depicted in Scheme 5.

The above described thio- and selenophosphinites could be obtained as analytically pure compounds. However, excess of phosphane sulfides and selenides as well as other proton sources had to be avoided to suppress dismutation into the corresponding dimesitylphosphinates and dimesitylphosphanides.

## NMR spectroscopy

Selected NMR parameters of compounds of the type Ar$_2$P(E)H and Ar$_2$PE-A(L)$_n$ (Ar = Ph, Mes; E = O, S, Se, A = Li, Na, K, L = ether base) are compared in Table 1. Increasing radius (and hence softness) of the chalcogen atom leads to higher frequency shifted $^{31}$P NMR resonances. Substitution of the phenyl substituents by bulkier mesityl groups causes a high field shift of the signals. Deprotonation of diarylphosphane oxides and hence formation of the alkali metal diarylphosphinites shifts the $^{31}$P resonances to lower field by approx. 60 ppm whereas chemical $^{31}$P shift differences are significantly smaller for the sulfur and selenium congeners. The influence of the aryl groups and the chalcogen atoms on the $^1J(^{31}P,^1H)$ coupling constants of Ar$_2$P(E)H is rather small and values around 465 Hz are observed. The $^1J(^{31}P,^{77}Se)$ coupling does also not depend on the substitution pattern of the aryl group. However, metalation of the diarylphosphane selenides and formation of the alkali metal selenophosphinites halves the values of these coupling constants. This finding can be expected because the P–Se bond lengths elongate upon deprotonation from 211.28(5) pm for **1b** to 223.29(8) and 223.88(6) pm for **2b** and **3b**, respectively. Generally, also $^1J(^{31}P,^1H)$ coupling constants in P$^{III}$ compounds with phosphorus atoms in pyramidal environments are much smaller than those values of P$^V$ congeners with tetrahedrally coordinated phosphorus atoms.

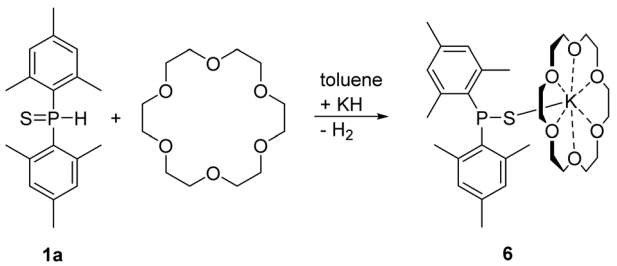


**Scheme 5** Synthesis of mononuclear [(18C6)K-SPMes$_2$] (**6**) *via* metalation of dimesitylphosphane sulfide (**1a**) with KH in toluene in the presence of [18]crown-6.

**Table 1** Comparison of $^{31}$P NMR chemical shifts as well as $^1J(^{31}P,^1H)$ and $^1J(^{31}P,^{77}Se)$ coupling constants

| E | O | S | Se[a] |
|---|---|---|---|
| Ph$_2$P(E)H[a] | 21.7 [17] | 20.9 (465)[18] | 5.64 (461) [−740][19] |
| Mes$_2$P(E)H[a] | 11.4 (481) | −1.5 (467) | −27.7 (461) [−726] |
| Li-EPPh$_2$ | 88.9 [10] | 20.7 [20] | 5.1 [−316][21] |
| Na-EPPh$_2$ | 90.5 [10] | 22.3 [20] | 6.8 [−360] |
| K-EPPh$_2$ | 86.8 [10] | 25,[20] 26.8[b] [8] | 9.7 [−377] |
| Li-EPMes$_2$ | —[c] [4] | 16.4 | −11.9 [−316] |
| Na-EPMes$_2$ | 101.5 [18] | 16.9 | −13.9 [−320] |
| K-EPMes$_2$ | 95.9 [8] | 21.0 | −8.9 [−351] |

[a] $^1J(^{31}P,^{77}Se)$ coupling constants are given in brackets, $^1J(^{31}P,^1H)$ values in parentheses. [b] Chemical shift of the tetrahydropyran adduct [(thp)KSPPh$_2$]$_\infty$. [c] No NMR data given due to decomposition according to Scheme 2.

## Molecular structures

For comparison reasons, the molecular structures of dimesitylphosphane sulfide (**1a**) and selenide (**1b**) have been determined. The molecular structure and atom labelling scheme of **1a** are depicted in Fig. 1, compound **1b** is shown in the ESI.† Selected bond lengths and angles are listed in Table 2. Due to a diminished electronegativity difference between P and E for the heavier chalcogens S and Se, the P–E bond becomes less heteropolar with decreasing positive character of the phosphorus atom.

The bond lengths of Mes$_2$P(E)H are very similar to those found for Ph$_2$P(E)H (E = O,[13] S,[8] Se[14]), a slight but systematic elongation of the P–C bonds is caused by bulkier mesityl substituents. The distortion of the tetrahedral environment of P1 is more striking with an increasing difference $\Delta$ between the proximal and distal E1–P1–C1/C10 bond angles for the heavier chalcogenides ($\Delta$ = 2.7° for O, 7.7° for S, 8.8° for Se) due to

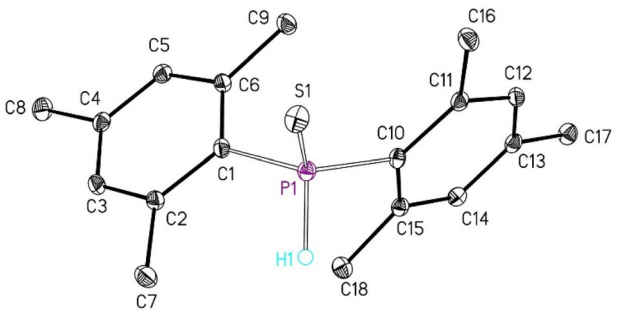


**Fig. 1** Solid state molecular structure and atom labelling scheme of Mes$_2$P(S)H (**1a**). The ellipsoids represent a probability of 30%, H atoms bound to C atoms are neglected for the sake of clarity. Selected bonding parameters are listed in Table 2.

**Table 2** Selected bond lengths (pm) and angles (°) of Mes$_2$P(E)H [E = O,[22] S (**1a**) and Se (**1b**)]

| E | O | S (**1a**) | Se (**1b**) |
|---|---|---|---|
| P1–E1 | 148.54(13) | 195.68(6) | 211.28(5) |
| P1–C1 | 181.51(18) | 182.34(17) | 182.91(13) |
| P1–C10 | 181.62(18) | 182.33(18) | 181.91(13) |
| C1–P1–C10 | 108.07(8) | 107.68(8) | 107.65(6) |
| E1–P1–C1 | 113.94(8) | 113.46(6) | 122.17(4) |
| E1–P1–C10 | 116.64(8) | 121.14(6) | 113.42(5) |

steric repulsion between an *ortho*-methyl substituent and the chalcogen atom.

Alkali metal diarylphosphinites crystallize preferably with tetranuclear structures with central $A_4O_4$ heterocubane cages as observed for lithium[6] and potassium.[8] Bidentate Lewis bases (like 1,2-dimethoxyethane and tmeda) stabilize dinuclear $[(dme)Li\text{-}OPPh_2]_2$[7] and $[(tmeda)Na\text{-}OPMes_2]_2$[23] with $A_2O_2$ rings. Crown ethers such as 18-crown-6 deaggregate the tetranuclear potassium cage compound and even mononuclear $[(18C6)K\text{-}OPAr_2]$ (Ar = Ph, Mes) crystallizes.[16] Substitution of the oxygen atom by sulfur in $[(thp)K\text{-}SPPh_2]_\infty$ changes the structure in the solid phase drastically and a wavy strand structure forms[8] whereas in $[(tmeda)Li\text{-}SPPh_2]_2$ the expected four-membered $Li_2S_2$ ring is observed.[24] However, the homologous dinuclear selenium congener $[(tmeda)Li\text{-}SePPh_2]_2$ shows a unique molecular structure and this derivative crystallizes with a five-membered $Li_2Se_2P$ ring.[25] Based on this diverse coordination chemistry of diaryl-chalcogenophosphinites, we became interested in the dimesityl derivatives with bulkier aryl substituents to elucidate structural and NMR spectroscopic trends in dependency of the chalcogen and alkali metal atoms as well as of the neutral co-ligand.

Molecular structures and atom labelling schemes of $[(thf)_2K\text{-}SPMes_2]_2$ (**2a**) and of $[(thp)_2K\text{-}SePMes_2]_2$ (**3b**) are depicted in Fig. 2 and 3, molecular structures of $[(thp)_2K\text{-}SPMes_2]_2$ (**3a**) and of $[(thf)_2K\text{-}SePMes_2]_2$ (**2b**) are shown in the ESI.† THF is a stronger Lewis base than THP but very similar aggregation degrees and discrete dinuclear molecules are observed.

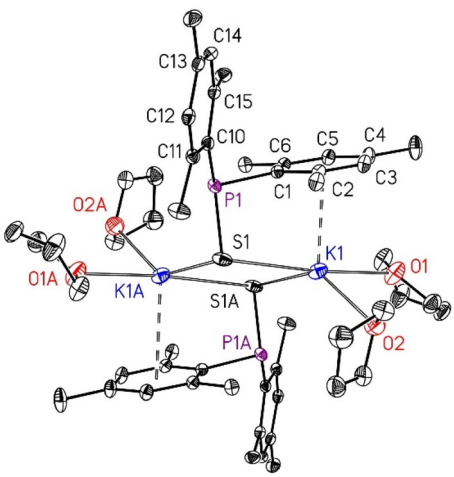


**Fig. 2** Solid state molecular structure and atom labelling scheme of centrosymmetric $[(thf)_2K\text{-}SPMes_2]_2$ (**2a**). The ellipsoids represent a probability of 30%, H atoms are omitted for clarity reasons. Symmetry-equivalent atoms are marked with the letter "A". Selected bond lengths (pm): K1–S1 323.71(7), K1–S1A 314.77(7), P1–S1 207.19(7), P1–C1 186.43(18), P1–C10 186.95(18), K1–O1 269.47(19), K1–O2 278.8(2); angles (°): C1–P1–C10 100.38(7), S1–P1–C1 99.98(6), S1–P1–C10 114.52(6), K1–S1–K1A 91.475(18), K1–S1–P1 95.03(2), K1A–S1–P1 86.42(2), S1–K1–S1A 88.525(18), S1–K1–O1 174.92(5), S1–K1–O2 97.54(4), S1A–K1–O1 94.53(4), S1A–K1–O2 139.51(5), O1–K1–O2 82.77(5).

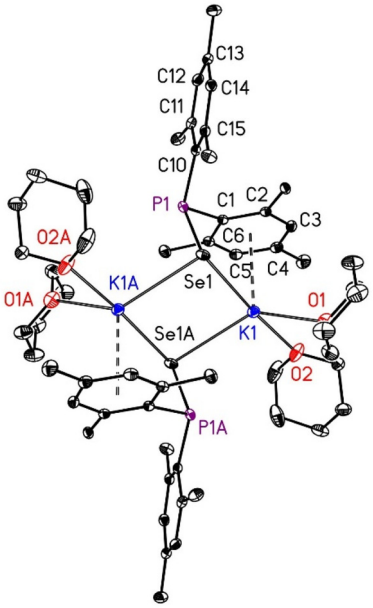


**Fig. 3** Solid state molecular structure and atom labelling scheme of centrosymmetric $[(thp)_2K\text{-}SePMes_2]_2$ (**3b**). The ellipsoids represent a probability of 30%, H atoms are neglected for the sake of clarity. Symmetry-related atoms are marked with the letter "A". Selected bond lengths (pm): K1–Se1 328.61(9), K1–Se1A 322.63(8), P1–Se1 223.88(6), P1–C1 186.57(15), P1–C10 186.82(15), K1–O1 272.35(15), K1–O2 264.59(15); angles (°): C1–P1–C10 102.42(7), Se1–P1–C1 98.68(5), Se1–P1–C10 114.85(5), K1–Se1–K1A 88.530(10), K1–Se1–P1 93.571(13), K1A–Se1–P1 89.51(2), Se1–K1–S1eA 91.471(10), Se1–K1–O1 93.80(3), Se1–K1–O2 175.80(4), Se1A–K1–O1 136.93(4), Se1A–K1–O2 92.57(4), O1–K1–O2 82.45(4).

Potassium dimesityl-chalcogenophosphinites have central $K_2E_2$ rings in common and two ether bases bind to the potassium ions. In addition, π-interactions to side-on bound aryl groups saturate the coordination spheres of the alkali metals, thus shielding one side of the Lewis-acidic cation and preventing aggregation to larger molecules or to coordination polymers. In addition, this coordination mode enforces significantly different proximal and distal E1–P1–C1/C10 bond angles. The smaller size of the $K_2S_2$ ring compared to the $K_2Se_2$ cycle enhances steric repulsion between the mesityl substituent and ligated ether molecules leading to larger K1–O1 and K1–O2 distances. In all potassium chalcogenophosphinites, two strongly different K1–O1 and K1–O2 bond lengths are observed due to repulsive forces between an *ortho*-methyl group and one of the ether bases.

In Table 3 selected bonding parameters of the dinuclear potassium dimesityl-chalcogenophosphinites of the type $[(L)_2K\text{-}EPMes_2]_2$ are compared. All these derivatives have nearly square $K_2E_2$ rings with slightly different K–E bond lengths. The coordination spheres are best described as square pyramidal environments, taking ligated π-bound aryl groups as single ligands. The *ortho*-methyl group of the side-on bound mesityl group pushes one ether base slightly out of the square $O_2E_2$ plane leading to an enhancement of the respective K1–O dis-

Table 3 Comparison of selected structural parameters [bond lengths (pm) and angles (°)] of dinuclear potassium dimesityl-chalcogenophosphinites $[(L)_2K\text{-}EPMes_2]_2$

| | 2a | 2b | 3a | 3b |
|---|---|---|---|---|
| E | S | Se | S | Se |
| L | thf | thf | thp | thp |
| K1–O1 | 269.5(2) | 275.1(2) | 284.4(2) | 272.4(2) |
| K1–O2 | 278.8(2) | 270.2(2) | 275.2(2) | 264.6(2) |
| K1–E1 | 323.71(7) | 334.96(7) | 312.30(11) | 328.61(9) |
| K1–E1A | 314.77(7) | 326.37(7) | 326.77(10) | 322.63(8) |
| K1–$C_{min}$ [a] | 313.4(2) | 314.5(3) | 315.6(3) | 319.2(2) |
| K1–$C_{max}$ [b] | (358.02) | 351.1(3) | 348.1(3) | 346.1(2) |
| Δ(K–C)[c] | 44.5 | 36.6 | 32.5 | 26.9 |
| ∑(E1)[d] | 272.9 | 273.1 | 270.1 | 271.6 |
| ∑(P1)[d] | 314.9 | 314.2 | 317.3 | 316.0 |
| E1–K1–E1A | 88.52(2) | 88.41(2) | 85.18(3) | 91.47(1) |
| K1–E1–K1A | 91.48(2) | 91.59(2) | 94.45(3) | 88.53(1) |
| O1–K1–O2 | 82.77(5) | 84.30(7) | 86.15(7) | 82.45(4) |

[a] Shortest potassium–carbon bond to the π-bound mesityl substituent. [b] Largest K–C distance to the π-bound mesityl substituent. [c] Difference between largest and smallest K–C bond lengths. [d] Angle sums of the chalcogen atom E1 and of the phosphorus atom P1.

tance. The larger P–Se and K–Se bond lengths offer more flexibility for the adjustment of the π-interaction between K1 and the aryl group, leading to smaller differences between K1–$C_{max}$ and K1–$C_{min}$ which is a measure for tilting of the mesityl group with respect to the K1 atom (or the dislocation of the potassium atom K1 from the center of the aromatic ring). It is obvious that the stronger thf ligand enhances the dislocation in comparison to the weaker thp bases.

The molecular structures and atom labelling schemes of centrosymmetric lithium (**4**) and sodium dimesityl-thiophosphinites (**5**) are depicted in Fig. 4 and 5. The structure of **4** is comparable to the O congener $[(dme)Li\text{-}OPPh_2]_2$ [7] with a central $Li_2E_2$ ring without any π-interactions to the aromatic aryl substituents. The lithium atoms are in distorted tetrahedral coordination environments with large S–Li1–O and smaller O1–Li1–O1 and S1–Li1–S1A bond angles. The Li1–O1 and Li1–O2 bond lengths have rather similar values but steric strain is minimized by tilting of the bridging thiophosphinite ligand leading to different S1–P1–C1 and S1–P1–C10 bond angles.

The molecular structure and atom labelling scheme of homologous $[(thf)_2Na\text{-}SPMes_2]_2$ (**5**) are depicted in Fig. 5. The thf ligand of O2 is disordered on two sites verifying reduced intramolecular steric pressure. Due to the larger radius of sodium ions ($r(Li^+)$ 73, $r(Na^+)$ 113, $r(K^+)$ 151 pm),[15] steric strain is released and very similar S1–P1–C1 and S1–P1–C10 bond angles exist. The smaller radii of lithium and sodium ions make these alkali metals rather hard Lewis acids preferring hard ether bases whereas for larger and softer potassium ions, the ether bases compete with the soft π-systems of the aryl groups.

Selected structural parameters of $[(thf)_2A\text{-}SPMes_2]_2$ with A = Li (**4**), Na (**5**) and K (**2a**) are compared in Table 4. The small radius of the lithium ion induces intramolecular steric repul-

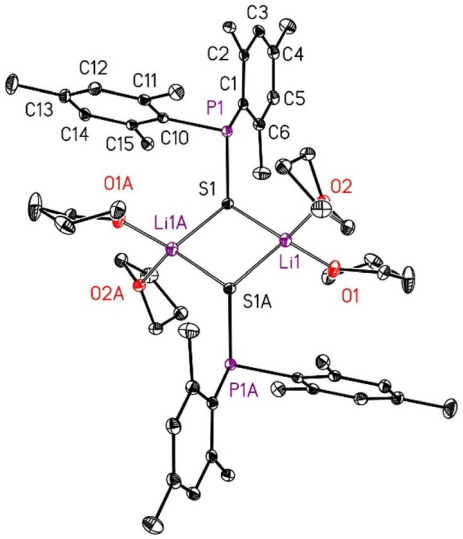


Fig. 4 Solid state molecular structure and atom labelling scheme of $[(thf)_2Li\text{-}SPMes_2]_2$ (**4**). The ellipsoids represent a probability of 30%, H atoms are omitted for clarity reasons. Symmetry-related atoms are marked with the letter "A". Selected bond lengths (pm): Li1–S1 245.8(2), Li1–S1A 248.8(2), P1–S1 207.51(5), P1–C1 186.46(12), P1–C10 186.24(12), Li1–O1 192.6(2), Li1–O2 194.0(2); angles (°): C1–P1–C10 102.08(5), S1–P1–C1 113.32(4), S1–P1–C10 102.60(4), Li1–S1–Li1A 79.49(8), Li1–S1–P1 111.53(6), Li1A–S1–P1 116.88(6), S1–Li1–S1A 100.52(8), S1–Li1–O1 108.47(10), S1–Li1–O2 121.77(11), S1A–Li1–O1 123.27(11), S1A–Li1–O2 101.18(10), O1–Li1–O2 103.05(11).

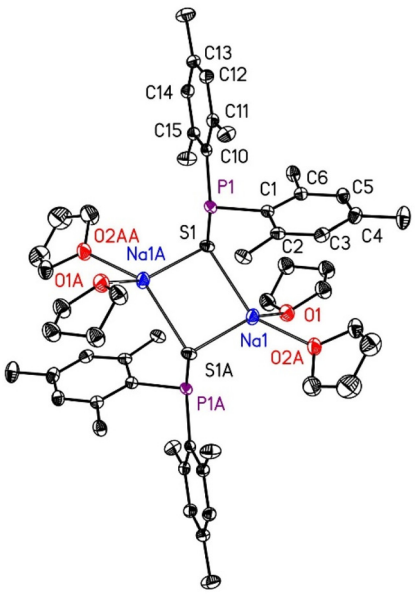


Fig. 5 Solid state molecular structure and atom labelling scheme of $[(thf)_2Na\text{-}SPMes_2]_2$ (**5**). The ellipsoids represent a probability of 30%, H atoms are omitted for clarity reasons. Disordering of O2 is not shown. Symmetry-equivalent atoms are marked with the letter "A". Selected bond lengths (pm): Na1–S1 281.95(13), Na1–S1A 284.11(13), Na1–P1A 314.15(13), P1–S1 207.32(9), P1–C1 185.4(2), P1–C10 186.6(2), Na1–O1 233.9(2), Na1–O2A 231.9(8), Na1–O2B 237.2(18); angles (°): C1–P1–C10 101.65(10), S1–P1–C1 113.52(8), S1–P1–C10 114.26(8), Na1–S1–Na1A 83.73(4), Na1–S1–P1 102.67(4), Na1A–S1–P1 77.74(4), S1–Na1–S1A 96.27(4), S1–Na1–O1 89.98(7), S1–Na1–O2A 149.1(2), S1A–Na1–O1 151.38(8), S1A–Na1–O2 101.61(18), O1–Na1–O2 86.24(18).

Table 4 Comparison of selected structural parameters [bond lengths (pm) and angles (°)] of $[(thf)_2A\text{-}SPMes_2]_2$ with A = Li (**4**), Na (**5**) and K (**2a**) and of $[(18C6)K\text{-}SPMes_2]$ (**6**)

| A | Li (**4**) | Na (**5**) | K (**2a**) | K (**6**) |
|---|---|---|---|---|
| P1–S1 | 207.51(5) | 207.32(9) | 207.19(7) | 205.11(7) |
| A1–S1 | 245.8(2) | 282.0(1) | 323.71(7) | 306.85(8) |
| A1–S1A | 248.8(2) | 284.1(1) | 314.77(7) | — |
| ∑(P1)[a] | 318.00 | 329.43 | 314.88 | 315.75 |
| S1–P1–C1 | 113.32(4) | 113.52(8) | 99.98(6) | 114.53(6) |
| S1–P1–C10 | 102.60(4) | 114.26(8) | 114.52(6) | 99.72(6) |
| C1–P1–C10 | 102.08(5) | 101.7(1) | 100.38(7) | 101.50(8) |
| ∑(S1)[b] | 307.90 | 264.14 | 272.93 | — |
| A1–S1–A1A | 79.49(8) | 83.73(4) | 91.48(2) | — |
| P1–S1–A1 | 111.53(6) | 102.67(4) | 95.03(2) | 101.91(3) |
| P1–S1–A1A | 116.88(6) | 77.74(4) | 86.42(2) | — |
| O1–A1–O2 | 103.1(1) | 86.2(2) | 82.77(5) | [c] |

[a] Angle sum of P1. [b] Angle sum of S1. [c] There are three groups of O–K–O bond angles: bite angles O($n$)–K1–O($n$ + 1) vary around 60°, O($n$)–K1–O($n$ + 2) bond angles around 120° and O($n$)–K1–O($n$ + 3) values around 160°.

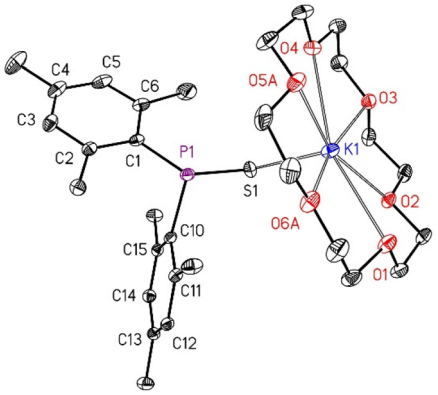


Fig. 6 Solid state molecular structure and atom labelling scheme of $[(18C6)K\text{-}SPMes_2]$ (**6**). The ellipsoids represent a probability of 30%, H atoms are omitted for clarity reasons. The disordering of the atoms O5A/B and O6A/B is not shown. Selected bond lengths (pm): K1–S1 306.85(8), P1–S1 205.11(7), P1–C1 186.7(2), P1–C10 186.2(2), K1–O1 293.3(1), K1–O2 276.9(1), K1–O3 284.4(2), K1–O4 280.7(2), K1–O5A 286(1), K1–O5B 289(2), K1–O6A 276.2(7), K1–O6B 273(2); bond angles (°): C1–P1–C10 101.50(8), S1–P1–C1 114.53(6), S1–P1–C10 99.72(6), K1–S1–P1 101.91(3), S1–K1–O1 114.14(4), S1–K1–O2 85.54(3), S1–K1–O3 80.92(3), S1–K1–O4 87.54(4), S1–K1–O5A 112.1(2), S1–K1–O5B 115.0(4), S1–K1–O6A 111.3(2), S1–K1–O6B 120.3(3).

sion leading to a large angle sum of S1. The larger Na–S distances release steric pressure, and a smaller ∑(S1) value can be realized and very similar S1–P1–C1 and S1–P1–C10 bond angles are found. Contrary to this finding, steric pressure is slightly enhanced in potassium derivative **2a** due to the enlarged coordination number by additional π-interactions to the mesityl rings, again giving an enlarged angle sum at S1 and quite different S1–P1–C1/C10 angles. The small radius of $Li^+$ also affects the O1–Li1–O2 bond angle due to steric repulsion between the thf ligands, whereas significantly smaller O1–A1–O1 values are observed for sodium (**5**) and potassium (**2a**).

The molecular structure and atom labelling scheme of $[(18C6)K\text{-}SPMes_2]$ (**6**) are depicted in Fig. 6. The crown ether hinders aggregation and hence a mononuclear complex is stabilized. In comparison to dinuclear $[(thf)_2K\text{-}SPMes_2]_2$ (**2a**), smaller K1–S1 and P1–S1 bond lengths are observed (Table 4).

In Table 4 selected structural parameters of the alkali metal dimesitylthiophosphinites of lithium, sodium, and potassium are compared. The phosphinite anion shows characteristic structural parameters with C1–P1–C10 bond angles slightly larger than 100° regardless of the alkali metal and of the bridging or terminal position but smaller than observed in $Mes_2P(S)H$ (**1a**, Table 2). Remarkably, the S1–P1–C1/C10 bond angles differ significantly regardless of the bridging or terminal binding mode as shown for the potassium derivatives **2a** and **6**. The exception is the sodium complex **5** with two rather large S1–P1–C1/C10 angles leading to an enhanced angle sum at P1 although the compounds **4** (A = Li), **5** (A = Na), and **2a** (A = K) crystallize as dimeric centrosymmetric molecules with tetracoordinate alkali metal atoms. However, in derivative **2a** one mesityl group shows interactions between the potassium atom and the π-system of one mesityl group. This side-on coordination mode of the aryl group leads to distortion of the four-membered $K_2S_2$ ring and different K1–S1 and K1–S1A bond lengths. In the sodium derivative **5** the metal-aryl interaction tilts the phosphinite anion and significantly different P1–S1–Na1/Na1A bond angles are observed. In addition, the angles within the phosphinite anion deviate from those of the other congeners and two quite similar S1–P1–C1/C10 bond angles are realized.

Concluding investigations concern the ability of the potassium dimesityl-chalcogenophosphinites to enable catalytic formation of dimesityl-alkenylphosphane oxides *via* addition of $Mes_2P(E)H$ onto alkynes. The potassium-mediated addition of dimesitylphosphane oxide across alkynes (Pudovik reaction) succeeds smoothly with good yields whereas lithium and sodium are unsuitable alkali metals to promote these addition reactions.[2] Contrary to this finding, substitution of E = O by the heavier chalcogens sulfur and selenium impedes this catalytic conversion. Several reasons may contribute to this finding:

(i) The heteropolar P–O bond leads to polarization and negatively charged oxygen sites on the one hand and positively charged P atoms on the other whereas the P-E bonds (E = S, Se) are mainly of covalent nature. The positively charged P atoms in $K\text{-}OPAr_2$ ease the attack at electron-rich unsaturated compounds such as alkynes and heterocumulenes.

(ii) The enhanced negative charge on the oxygen base enables strong electrostatic bonds to cations whereas the soft and large chalcogen bases can compete with the soft aromatic π-systems. The potassium π-interactions strongly shield the reactive sites of the complexes $K\text{-}EPAr_2$ with E = S, Se.

(iii) The dismutation rate of $K\text{-}E\text{-}PMes_2$ (E = S, Se) into the corresponding phosphinates $KE_2PMes_2$ and phosphanides $KPMes_2$ is accelerated in the presence of weak proton sources (Brønsted acids) such as $R_2P(E)H$ leading to a decline of the catalyst.

Consequently, alternative routes must be chosen to prepare diaryl-alkenylphosphane sulfides and selenides. A feasible strategy involves several steps, including the Pudovik reaction and synthesis of diaryl-alkenylphosphane oxides, subsequent reduction of these compounds to phosphanes and finally, sulfurization or selenation with the heavy elemental chalcogens.

# Experimental

### General information

All manipulations were carried out under an inert nitrogen atmosphere using standard Schlenk techniques. The solvents were dried over KOH and subsequently distilled over sodium/benzophenone under a nitrogen atmosphere prior to use. All substrates were purchased from Alfa Aesar, abcr, Sigma Aldrich or TCI and used without further purification. $Mes_2PH$ was prepared by an adjusted literature procedure.[26] The yields given are not optimized. Purity of the compounds was verified by NMR spectroscopy. Deuterated solvents were dried over sodium, distilled, degassed, and stored under nitrogen over sodium. $^1$H, $^{13}$C{$^1$H}, and $^{31}$P NMR spectra were recorded on Bruker Avance I 250 (BBO) Bruker Avance III 400 (BBO, BBFO probes), Avance neo 500 (BBFO Prodigy probe), and Avance III HD 600 (TCI cryoprobe) spectrometers. Chemical shifts ($^1$H, $^{13}$C) are reported in parts per million relatively to $SiMe_4$ as an external standard referenced to the solvents residual proton signal using xiref AU program for $^{13}$C NMR spectra. The assignment of the NMR signals is depicted in Scheme 6. DOSY-NMR spectra were measured using the convection compensated dstebpgp3s standard pulse sequence. ASAP-HSQC spectra and ASAP-HSQC-DEPT spectra were recorded using the published pulse sequences.[27] Elemental analyses of the alkali metal compounds gave no reproducible and reliable results due to loss of ligated ether bases and formation of carbonates during handling and combustion. During heating and combustion analysis, small amounts of **1a** and **1b** degraded and sublimed; this led to generally too small values and has been taken into account by adjusting the elemental analysis according to the H values.

### Synthesis of $Mes_2P(S)H$ (1a)

The suspension of dimesitylphosphane oxide (302 mg, 1.1 mmol, 1.0 equiv.) and 2,4-bis(4-methoxyphenyl)-1,3,2,4-dithiadiphosphetane-2,4-disulfide (Lawessons reagent, 191 mg, 0.47 mmol, 0.4 equiv.) in 10 mL of THF was heated under reflux for 2 h. During this time a slightly yellow clear solution formed. Then the solvent was removed *in vacuo* and the residue recrystallized from acetonitrile (6 mL), yielding dimesitylphosphane sulfide (**1a**) as a colorless solid (119 mg, 40%), mp: 152–156 °C (dec.). $^1$H NMR (400.13 MHz, $CDCl_3$, 298 K): $\delta$ = 8.52 (d, 1H, $^1J_{PH}$ = 471.8 Hz, H–P), 6.86 (d, 4H, $^4J_{PH}$ = 4.4 Hz, H3), 2.49 (s, 12H, H5), 2.27 (s, 6H, H6). $^{31}$P NMR ($CDCl_3$, 161.98 MHz, 298 K): $\delta$ = −1.45 (d, $^1J_{PH}$ = 468.6 Hz). $^{13}$C{$^1$H} NMR ($CDCl_3$, 100.61 MHz, 298 K): $\delta$ = 141.7 (d, $^5J_{PC}$ = 3.3 Hz, C4), 141.4 (d, $^2J_{PC}$ = 10.5 Hz, C2), 131.1 (d, $^3J_{PC}$ = 10.9 Hz, C3), 125.6 (d, $^1J_{PC}$ = 81.1 Hz, C1), 21.3 (d, $^3J_{CP}$ = 8.8 Hz, C5), 21.2 (s, C6). MS (*m*/*z*): 325 $[M + Na]^+$, 303 $[M + H]^+$. Elemental analysis: found: C 71.07, H 7.67, S 9.80; calc. for $C_{18}H_{23}PS$: C 71.49, H 7.67, S 10.60; IR (ATR, $cm^{-1}$): 2913 (m), 2378 (m), 1601 (s), 1447 (s), 673 (vs), 630 (s).

### Synthesis of $Mes_2P(Se)H$ (1b)

Dimesitylphosphane (2.72 g, 10 mmol, 1.0 equiv.) and grey selenium granules (797 mg, 10 mmol, 1.0 equiv.) were heated under reflux in 15 mL of toluene for 4 h. Unreacted selenium was removed by filtration and thereafter the solvent was removed by distillation *in vacuo*. The residue was heated under reflux in *n*-hexane for 2 h. Then the product dimesitylphosphane selenide (**1b**, 1.26 g, 36%) was collected by filtration. This compound was a colorless solid which quickly degraded under aerial conditions. $^1$H NMR (400.13 MHz, $C_6D_6$, 298 K): $\delta$ = 8.09 (d, 1H, $^1J_{PH}$ = 463 Hz, P–H), 6.53 (d, 4H, $^3J_{PH}$ = 4 Hz, H3), 2.44 (s, 12H, H5), 1.97 (s, 6H, H6). $^{31}$P NMR (161.98 MHz, $C_6D_6$, 298 K): $\delta$ = −27.7 (d, $^1J_{PH}$ = 461 Hz, satellites $^1J_{PSe}$ = 726 Hz). $^{13}$C{$^1$H} NMR (100.61 MHz, $C_6D_6$, 298 K): $\delta$ = 141.7 (d, $^2J_{PC}$ = 10.1 Hz, C2), 141.2 (d, $^4J_{PC}$ = 3.4 Hz, C4), 131.2 (d, $^3J_{PC}$ = 10.3 Hz, C3), 124.6 (d, $^1J_{PC}$ = 71.6 Hz, C1), 21.4 (d, $^3J_{PC}$ = 8.5 Hz, C5), 20.9 (s, C6). $^{77}$Se NMR (76.31 MHz, $C_6D_6$, 298 K): $\delta$ = −274.12 (d, $^1J_{PSe}$ = 726 Hz). MS (*m*/*z*): 373 $[M + Na]^+$, 351 $[M + H]^+$, 349 $[M - H]^+$. Elemental analysis: calcd: C 61.89, H 6.64; found: C 61.77, H 6.64. IR (ATR, $cm^{-1}$): 2912 (w), 2387 (w), 1601 (m), 1442 (s), 843 (s), 622 (vs), 553 (vs), 492 (vs). Dec. above 130 °C (without melting).

### Synthesis of $[(thf)_2K\text{-}SPMes_2]_2$ (2a)

Potassium hydride (300 mg, 7.5 mmol, 4.3 equiv.) and $Mes_2P(=S)H$ (527 mg, 1.74 mmol, 1.0 equiv.) were combined in a Schlenk flask and cooled to −20 °C. Then 20 mL of THF were added and the suspension stirred for 2.5 h whereat a yellow solution formed. Then the volume of the solution was reduced to a third of the original volume and stored at −20 °C yielding yellow crystalline **2a** (yield: 444 mg, 52%). $^1$H NMR (400.13 MHz, THF-$d_8$, 253 K): $\delta$ = 6.52 (s, 8H, H3), 2.49 (s, 24H, H5), 2.09 (s, 12H, H6). $^{31}$P NMR (161.98 MHz, THF-$d_8$, 253 K): $\delta$ = 21.0 (s). $^{13}$C{$^1$H} NMR (100.61 MHz, THF-$d_8$, 253 K): $\delta$ = 143.8 (d, $^1J_{CP}$ = 50.2 Hz, C1), 141.5 (d, $^2J_{CP}$ = 15.0 Hz, C2), 134.7 (s, C4), 129.8 (s, C3), 22.6 (d, $^3J_{CP}$ = 16.4 Hz, C5), 20.8 (s, C6). IR (ATR, $cm^{-1}$): 2919 (m), 1601 (m), 1445 (s), 1055 (s), 1025 (s), 846 (s), 632 (vs). Dec. above 245 °C (without melting).

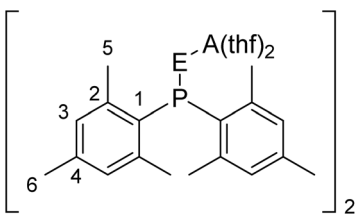


**Scheme 6** Atom labelling scheme for the assignment of the NMR signals.

### Synthesis of $[(thf)_2K\text{-}SePMes_2]_2$ (2b)

A solution of $Mes_2P(Se)H$ (171 mg, 0.5 mmol, 1.0 equiv.) in 10 mL of THF was added at −40 °C to a suspension of potassium hydride (33 mg, 0.8 mmol, 1.6 equiv.) in THF. Hydrogen gas was liberated, and the suspension turned yellow. After four hours of stirring the volume of the solution was reduced to half of the original volume. During storage at −20 °C a few yellow crystals of **2b** precipitated (yield was approx. 5%). $^1$H NMR (400.13 MHz, THF-$d_8$, 253 K): $\delta$ = 6.58 (s, 8H, H3), 2.54 (s, 24H, H5), 2.16 (s, 12H, H6). $^{31}$P NMR (161.98 MHz, THF-$d_8$, 253 K): $\delta$ = −8.9 (s, satellites $^1J_{PSe}$ = 350.8 Hz). $^{77}$Se NMR (76.31 MHz, THF-$d_8$, 253 K): $\delta$ = −167.4 (d, $^1J_{PSe}$ = 354.3 Hz). IR (ATR, cm$^{-1}$): 2919 (m), 1601 (m), 1445 (s), 1055 (s), 847 (s). Dec. above 120 °C (without melting).

### Synthesis of $[(thp)_2K\text{-}SPMes_2]_2$ (3a)

Potassium hydride (364 mg, 9.1 mmol, 3.5 equiv.) was suspended in 5 mL of THP and cooled to −30 °C. Then dimesitylphosphane sulfide (791 mg, 2.6 mmol, 1.0 equiv.), dissolved in 20 mL of THP, was added dropwise within 15 min. The solution turned yellow and hydrogen gas evolved. The reaction mixture was stirred for 3 h and then all solids were removed by filtration. The volume of the solution was reduced and at −20 °C yellow $[K(SPMes_2)(thp)_2]_2$ (**3a**) crystallized (yield: 234 mg, 24%). $^1$H NMR (400.13 MHz, THF-$d_8$, 253 K): $\delta$ = 6.60 (s, 8H, H3), 3.57 (s, 5H, H7), 2.52 (s, 24H, H5), 2.12 (s, 12H, H6), 1.60 (d, 8H, H9), 1.49 (m, 16H, H8). $^{31}$P NMR (161.98 MHz, THF-$d_8$, 253 K): $\delta$ = 19.4 (s). $^{13}$C{$^1$H} NMR (100.61 MHz, THF-$d_8$, 253 K): $\delta$ = 143.5 (d, $^1J_{CP}$ = 50.3 Hz, C1), 141.5 (d, $^2J_{CP}$ = 15.6 Hz, C2), 134.8 (s, C4), 129.9 (s, C3), 68.8 (s, C7), 27.4 (s, C8), 24.3 (s, C9), 22.6 (d, $^3J_{CP}$ = 17.3 Hz, C5), 20.8 (s, C6). IR (ATR, cm$^{-1}$): 2919 (s), 1600 (m), 1441 (s), 1087 (s), 844 (s), Dec. above 287 °C (without melting).

### Synthesis of $[(thp)_2K\text{-}SePMes_2]_2$ (3b)

Potassium hydride (100 mg, 2.5 mmol, 1.9 equiv.) was placed in a flask at −30 °C and dimesitylphosphane selenide (470 mg, 1.3 mmol, 1.0 equiv.), dissolved in THP (21.5 mL), was added within 5 min. Evolution of hydrogen gas and formation of a yellow solution was observed. The reaction mixture was stirred for 2 h and then half of the solvent was removed *in vacuo*. At −20 °C yellow crystalline $[K(SePMes_2)(thp)_2]_2$ crystallized (yield: 273 mg, 30%). $^1$H NMR (400.13 MHz, THF-$d_8$, 253 K): $\delta$ (ppm) = 6.54 (s, 8H, H3), 3.53 (s, 6H, H7), 2.49 (s, 24H, H5), 2.12 (s, 12H, H6), 1.60 (d, 3H, H9), 1.49 (m, 6H, H8). $^{31}$P NMR (161.98 MHz, THF-$d_8$, 253 K): $\delta$ (ppm) = −10.5 (s, satellites $^1J_{PSe}$ = 353.1 Hz). $^{13}$C NMR (100.61 MHz, THF-$d_8$, 253 K): $\delta$ (ppm) = 141.7 (d, $^1J_{CP}$ = 52.9 Hz, C1), 141.7 (d, $^2J_{CP}$ = 14.7 Hz, C2), 134.6 (s, C4), 129.7 (s, C3), 68.8 (s, C7), 27.4 (s, C8), 24.3 (s, C9), 23.0 (d, $^3J_{CP}$ = 16.5 Hz, C5), 20.8 (s, C6). $^{77}$Se NMR (76.31 MHz, THF-$d_8$, 253 K): $\delta$ (ppm) = −166.4 (d, $^1J_{PSe}$ = 353.1 Hz). IR (ATR, cm$^{-1}$): 2918 (m), 1603 (m), 1402 (m), 1172 (m), 1086 (s), 645 (s).

### Synthesis of $[(thf)_2Li\text{-}SPMes_2]_2$ (4)

Dimesitylphosphane sulfide (496 mg, 1.6 mmol, 1.0 equiv.) was dissolved in THF (5 mL) and a solution of *n*BuLi (1.6 M, 1.1 ml, 1.1 equiv.) in *n*-heptane was added dropwise. The yellow solution was cooled to −20 °C, stirred for 2 h and then the volume of the solution was reduced to half of the original volume. Yellow crystalline $[Li(SPMes_2)(thf)_2]_2$ (**4**) precipitated during storage at −20 °C (yield: 152 mg, 21%). $^1$H NMR (400.13 MHz, THF-$d_8$, 253 K): $\delta$ = 6.49 (s, 8H, H3), 2.47 (s, 24H, H5), 2.08 (s, 12H, H6). $^{31}$P NMR (161.98 MHz, THF-$d_8$, 253 K): $\delta$ = 16.4 (s). $^{13}$C{$^1$H} NMR (100.61 MHz, THF-$d_8$, 253 K): $\delta$ = 143.2 (d, $^1J_{CP}$ = 50.3 Hz, C1), 141.7 (d, $^2J_{CP}$ = 15.6 Hz, C2), 134.5 (s, C4), 129.7 (s, C3), 22.6 (d, $^3J_{CP}$ = 16.5, C5), 20.8 (s, C6). $^7$Li NMR (155.51 MHz, THF-$d_8$, 253 K): $\delta$ = 0.36. IR (ATR, cm$^{-1}$): 2918 (m), 1602 (m), 1444 (s), 1053 (s), 622 (vs). Dec. above 190 °C (without melting).

### Synthesis of $[(thf)_2Na\text{-}SPMes_2]_2$ (5)

Sodium hydride (62 mg, 2.6 mmol, 1.1 equiv.) was placed in a Schlenk flask and dimesitylphosphane sulfide (706 mg, 2.3 mmol, 1.0 equiv.), dissolved in 7 mL of THF, was added. After gas evolution ceased, the solution was concentrated and cooled to −20 °C. At −20 °C yellow crystalline $[Na(SPMes_2)(thf)_2]_2$ (**5**) precipitated (yield: 436 mg, 40%). $^1$H NMR (400.13 MHz, THF-$d_8$, 253 K): $\delta$ (ppm) = 6.54 (s, 8H, H3), 2.51 (s, 24H, H5), 2.12 (s, 12H, H6). $^{31}$P NMR (161.98 MHz, THF-$d_8$, 253 K): $\delta$ (ppm) = 16.9 (s). $^{13}$C NMR (100.61 MHz, THF-$d_8$, 253 K): $\delta$ (ppm) = 143.0 (d, $^1J_{CP}$ = 49.4 Hz, C1), 141.6 (d, $^2J_{CP}$ = 14.7 Hz, C2), 134.7 (s, C4), 129.8 (s, C3), 22.6 (d, $^3J_{CP}$ = 17.3 Hz, C5), 20.8 (s, C6). IR (ATR, cm$^{-1}$): 2918 (m), 1602 (m), 1444 (s), 1053 (s), 847 (s), 636 (vs). Dec. above 170 °C (without melting).

### Synthesis of $[(18C6)K\text{-}SPMes_2]$ (6)

Dimesitylphosphane sulfide (**1a**, 486 mg, 1.6 mmol, 1.0 equiv.) in 10 mL of toluene was added dropwise at room temperature to a suspension of KH (99 mg, 2.5 mmol, 1.6 equiv.) and [18] crown-6 (429 mg, 1.6 mmol, 1.0 equiv.) in 10 mL of toluene. After one hour all solids were removed by filtration. The filtrate was cooled to −20 °C yielding 350 mg of yellow crystals of **6** (0.6 mmol, 38%). $^1$H NMR (400.13 MHz, THF-$d_8$, 253 K): $\delta$ (ppm) = 6.49 (s, 4H, H3), 3.55 (s, 24H, H7), 2.54 (s, 12H, H5), 2.10 (s, 6H, H6). $^{31}$P NMR (161.98 MHz, THF-$d_8$, 253 K): $\delta$ (ppm) = 24.3 (s). $^{13}$C{$^1$H} NMR (100.61 MHz, THF-$d_8$, 253 K): $\delta$ (ppm) = 145.6 (d, $^1J_{CP}$ = 53.8 Hz, C1), 141.8 (d, $^1J_{CP}$ = 14,7 Hz, C2), 133.8 (s, C4), 129.6 (s, C3), 71.0 (s, C7), 22.8 (d, $^1J_{CP}$ = 16.5 Hz, C5), 21.0 (s, C6). IR (ATR, cm$^{-1}$): 2886 (m), 1468 (m), 1451 (m), 1349 (s) 1102 (s), 960 (s), 835 (s), 641 (s). Dec. above 230 °C (without melting).

### Crystal structure determinations

The intensity data for the compounds were collected on a Nonius KappaCCD diffractometer equipped with a Mo-$K_\alpha$ IμS microfocus source and an Apex2 detector. Data were corrected for Lorentz and polarization effects; absorption was taken into account on a semi-empirical basis using multiple-scans.[28–31]

The structures were solved by intrinsic phasing methods (SHELXT-2018)[32] and refined by full-matrix least squares techniques against $F_o^2$ (SHELXL-2018).[33] The hydrogen atoms bonded to the phosphorus atom P1 of **1a** and **1b** were located by difference Fourier synthesis and refined isotropically. All other hydrogen atoms were included at calculated positions with fixed thermal parameters. All non-hydrogen atoms were refined anisotropically.[33] Crystallographic data as well as structure solution and refinement details are summarized in Table S1.† XP[34] and POV-Ray[35] were used for structure representations.

## Conclusions

Metalation of dimesitylphosphane sulfide (**1a**) and homologous selenide (**1b**) with *n*-butyllithium, NaH, and KH yields the following dinuclear complexes of the type $[(L)_2A\text{-}S\text{-}PMes_2]_2$ depending on the solvent: A = Li: L = thf (**4**); A = Na: L = thf (**5**); A = K: L = thf (**2a**), thp (**3a**) as well as $[(L)_2K\text{-}Se\text{-}PMes_2]_2$ with L = thf (**2b**), thp (**3b**). Deaggregation occurs in the presence of 18-crown-6 ether and mononuclear $[(18C6)K\text{-}S\text{-}PMes_2]$ forms. The preferential formation of dinuclear complexes with monodentate Lewis bases is in contrast to the tetranuclear potassium dimesitylphosphinites $[(L)K\text{-}O\text{-}PMes_2]_4$ with a central $K_4O_4$ heterocubane-type cage. These dimesityl-thiophosphinites and -selenophosphinites degrade into the corresponding phosphinates $AE_2PMes_2$ and phosphanides $APMes_2$; this degradation is accelerated in the presence of weak Brønsted acids. This behavior hampers the application of these compounds as catalysts in the Pudovik reaction, *i.e.* the addition of $Mes_2P(E)H$ onto alkynes.

These properties which are strikingly deviating from those of the lighter homologous phosphinites $A\text{-}O\text{-}PMes_2$ have several reasons. The phosphinites $A\text{-}O\text{-}PMes_2$ contain the hard and negatively charged oxygen base which can easily displace ether bases. Contrary, the soft and significantly less electronegative sulfur and selenium bases are significantly less basic and especially for the hard lithium cation coordination of neutral oxygen or nitrogen coligands is beneficial. For the softer potassium cation, coordination of the soft π-system of the mesityl groups can compete with the heavier chalcogen bases of the thio- and selenophosphinites.

## Author contributions

R. C. C. D.: Conceptualization, data analysis and methodology, data acquisition, writing original draft and editing; P. L. and H. G.: X-ray structure determinations at single crystals and editing of manuscript; M. W.: conceptualization and supervision, writing original draft and editing.

## Conflicts of interest

There are no conflicts to declare.

## Acknowledgements

We acknowledge the valuable support of the NMR and MS service platforms (**https://www.nmr.uni-jena.de**; **https://www.ms.uni-jena.de**) of the Faculty of Chemistry and Earth Sciences of the Friedrich Schiller University Jena, Germany.

## References

1 Z.-Y. Wang, Q. Guo, S. Xu and K.-K. Wang, *Synthesis*, 2021, 3683–3698.
2 B. E. Fener, P. Schüler, N. Ueberschaar, P. Bellstedt, H. Görls, S. Krieck and M. Westerhausen, *Chem. – Eur. J.*, 2020, **26**, 7235–7243.
3 A. W. J. Platten, A. M. Borys and E. Hevia, *ChemCatChem*, 2022, **14**, e202101853.
4 M. A. Beswick, N. L. Cromhout, C. N. Harmer, J. S. Palmer, P. R. Raithby, A. Steiner, K. L. Verhorevoort and D. S. Wright, *Chem. Commun.*, 1997, 583–584.
5 D. Martin, D. Moraleda, T. Achard, L. Giordano and G. Buono, *Chem. – Eur. J.*, 2011, **17**, 12729–12740.
6 (*a*) A. J. Hoskin and D. W. Stephan, *Organometallics*, 1999, **18**, 2479–2483; (*b*) C. Berthold, L. R. Thomas-Hargreaves, S. I. Ivlev and M. R. Buchner, *Z. Naturforsch.*, 2021, **76b**, 651–658.
7 M. Westerhausen, *Monolithiumphosphid·DME und -arsenid·DME – wertvolle Edukte für die Synthese von Acylphosphanen und -arsanen und verwandten Verbindungen*, Ph.D. thesis, Marburg/Lahn, Germany, 1987.
8 S. M. Härling, H. Görls, S. Krieck and M. Westerhausen, *Inorg. Chem.*, 2016, **55**, 10741–10750.
9 L. Horner, P. Beck and V. G. Toscano, *Chem. Ber.*, 1961, **94**, 1317–1322.
10 K. Issleib, B. Walther and E. Fluck, *Z. Chem.*, 1968, **8**, 67.
11 K. Goda, H. Gomi, M. Yoshifuji and N. Inamoto, *Bull. Chem. Soc. Jpn.*, 1977, **50**, 545–546.
12 B. Bildstein and F. Sladky, *Phosphorus, Sulfur Silicon Relat. Elem.*, 1990, **47**, 341–347.
13 S. Härling, J. Greiser, T. M. A. Al-Shboul, H. Görls, S. Krieck and M. Westerhausen, *Aust. J. Chem.*, 2013, **66**, 1264–1273.
14 F. Dornhaus, H.-W. Lerner and M. Bolte, *Acta Crystallogr., Sect. E: Struct. Rep. Online*, 2007, **63**, o4917.
15 A. F. Holleman, E. Wiberg and N. Wiberg, *Inorganic Chemistry*, Academic Press, San Diego, 1995.
16 S. M. Härling, S. Krieck, H. Görls and M. Westerhausen, *Inorg. Chem.*, 2017, **56**, 9255–9263.
17 T. L. Gianetti, R. E. Rodriguez-Lugo, J. R. Harmer, M. Trincado, M. Vogt, G. Santiso-Quinones and H. Grützmacher, *Angew. Chem., Int. Ed.*, 2016, **55**, 15323–15328.
18 D. Semenzin, G. Etemad-Moghadam, D. Albouy, O. Diallo and M. Koenig, *J. Org. Chem.*, 1997, **62**, 2414–2422.
19 M. McFarlane and D. S. Rycroft, *J. Chem. Soc., Chem. Commun.*, 1972, 902–903.
20 G. Koshiro, G. Hideyuki, Y. Masaaki and I. Naoki, *Bull. Chem. Soc. Jpn.*, 1977, **50**, 545–546.

21 R. P. Davies and M. G. Martinelli, *Inorg. Chem.*, 2002, **41**, 348–352.
22 A. J. Veinot, K. Ramgoolam, N. A. Giffin and J. D. Masuda, *Molbank*, 2017, **2017**, M957.
23 S. M. Härling, *s-Block-Metall-vermittelte Hydrophosphoranylierung von Heterokumulenen und Alkinen*, Ph.D. thesis, Jena/Germany, 2018. Structural data of centrosymmetric $[(tmeda)Na\text{-}OPMes_2]_2$: P–O 156.39(15), P–C 186.88(19) and 187.2(2), av. Na–O 224.2 pm, C–P–C 100.32 (8)°; molecular structure and atom labelling scheme are depicted in the ESI.† Crystallographic and refinement data have been deposited at the Cambridge Crystallographic Data Centre under CCDC 2184163.†
24 N. E. Mansfield, M. P. Coles and P. B. Hitchcock, *Phosphorus, Sulfur Silicon Relat. Elem.*, 2008, **183**, 2685–2702.
25 R. P. Davies and M. G. Martinelli, *Inorg. Chem.*, 2002, **41**, 348–352.
26 C. Bianchini, G. Lenoble, W. Oberhauser, S. Parisel and F. Zanobini, *Eur. J. Inorg. Chem.*, 2005, **23**, 4794–4800.
27 (*a*) D. Schulze-Sünninghausen, J. Becker, M. R. M. Koos and B. Luy, *J. Magn. Reson.*, 2017, **281**, 151–161; (*b*) D. Schulze-Sünninghausen, J. Becker and B. Luy, *J. Am. Chem. Soc.*, 2014, **136**, 1242–1245.
28 R. Hooft, *COLLECT, Data Collection Software*, Nonius B.V., Netherlands, 1998.
29 Z. Otwinowski and W. Minor, Processing of X-Ray Diffraction Data Collected in Oscillation Mode, in *Methods in Enzymology*, ed. C. W. Carter and R. M. Sweet, Macromolecular Crystallography, Part A, Academic Press, San Diego, USA, 1997, vol. 276, pp. 307–326.
30 (*a*) *SADABS 2.10*, Bruker-AXS Inc., Madison, WI, USA, 2002; (*b*) L. Krause, R. Herbst-Irmer, G. M. Sheldrick and D. Stalke, SADABS 2016/2, *J. Appl. Crystallogr.*, 2015, **48**, 3–10.
31 *Bruker APEX3 Bruker AXS LLC*, Madison, WI, USA, 2020.
32 G. M. Sheldrick, *Acta Crystallogr., Sect. A: Found. Adv.*, 2015, **71**, 3–8.
33 G. M. Sheldrick, *Acta Crystallogr., Sect. C: Struct. Chem.*, 2015, **71**, 3–8.
34 XP, Siemens Analytical X-ray Instruments Inc., Karlsruhe, Germany, 1990; Madison, WI, USA, 1994.
35 *POV-Ray, Persistence of Vision Raytracer*, Victoria, Australia, 2007.